Inorg. Chem. **2004**, *43*, 6313–6323

Synthesis and Evaluation of a High Relaxivity Manganese(II)-Based MRI Contrast Agent

Jeffrey S. Troughton,[†] Matthew T. Greenfield,[†] Jaclyn M. Greenwood,[†] Stéphane Dumas,[†] Andrea J. Wiethoff,[†] Jufeng Wang,[†] Marga Spiller,[‡] Thomas J. McMurry,[†] and Peter Caravan*[,†]

EPIX Medical Inc., 71 Rogers Street, Cambridge, Massachusetts 02142, and Department of Radiology, New York Medical College, Valhalla, New York 10595

Received April 4, 2004

The manganese(II) ion has many favorable properties that lead to its potential use as an MRI contrast agent: high spin number, long electronic relaxation time, labile water exchange. The present work describes the design, synthesis, and evaluation of a novel Mn(II) complex (**MnL1**) based on EDTA and also contains a moiety that noncovalently binds the complex to serum albumin, the same moiety used in the gadolinium based contrast agent MS-325. Ultrafiltration albumin binding measurements (0.1 mM, pH 7.4, 37 °C) indicated that the complex binds well to plasma proteins (rabbit: 96 ± 2% bound, human: 93 ± 2% bound), and most likely to serum albumin (rabbit: 89 ± 2% bound, human 98 ± 2% bound). Observed relaxivities (± 5%) of the complex were measured (20 MHz, 37 °C, 0.1 mM, pH 7.4) in HEPES buffer ($r_1 = 5.8$ mM^{-1} s^{-1}), rabbit plasma ($r_1 = 51$ mM^{-1} s^{-1}), human plasma ($r_1 = 46$ mM^{-1} s^{-1}), 4.5% rabbit serum albumin ($r_1 = 47$ mM^{-1} s^{-1}), and 4.5% human serum albumin ($r_1 = 48$ mM^{-1} s^{-1}). The water exchange rate was near optimal for an MRI contrast agent ($k^{298} = 2.3 \pm 0.9 \times 10^8$ s^{-1}). Variable temperature NMRD profiles indicated that the high relaxivity was due to slow tumbling of the albumin-bound complex and fast exchange of the inner sphere water. The concept of a high relaxivity Mn(II)-based contrast agent was validated by imaging at 1.5T. In a rabbit model of carotid artery injury, **MnL1** clearly delineated both arteries and veins while also distinguishing between healthy tissue and regions of vessel damage.

Introduction

Magnetic resonance imaging (MRI) is a widespread diagnostic tool in medicine that provides noninvasive high-resolution images of body tissues. Clinical MRI measures the NMR signal of protons, largely those of water. Differences in signal intensity create contrast in the image and may allow discrimination between tissue types and disease states. There are different mechanisms to create contrast in an image. The simplest is the difference in hydrogen concentration among tissues. However, contrast can also be created by weighting the imaging sequence to display differences in proton relaxation rates ($1/T_1$ and $1/T_2$), differences in chemical shift, differences in water diffusion, the effect of flowing blood, or by using magnetization transfer techniques.[1] In T_1-weighted imaging, a more intense signal is observed in regions where the longitudinal relaxation rate is fast (where T_1 is short). The longitudinal relaxation rate of water protons can be further enhanced by the addition of paramagnetic metal complexes. These complexes, known as MRI contrast agents,[2] provide enhanced image contrast in regions where the complex localizes.

There are several compounds approved for clinical use, and more are undergoing clinical trials. The first generation of contrast agents distribute to plasma and to the extracellular space.[3] Subsequent development focused on targeting tissue such as the liver and body fluids such as the blood pool.[4] At the pre-clinical stage, much effort is focused on "molecular imaging",[5] for example by targeting contrast agents to the $\alpha_v\beta_3$ integrin[6] associated with angiogenesis or to fibrin[7]

* To whom correspondence should be addressed. E-mail: pcaravan@epixmed.com. Fax: +1 617 250 6127.
† EPIX Medical Inc.
‡ New York Medical College.

(1) Edelman, R. R.; Hesselink, J. R.; Zlatkin, M. B. *MRI: Clinical Magnetic Resonance Imaging*; 2nd ed.; Saunders: Philadelphia, 1996.
(2) Caravan, P.; Ellison, J. J.; McMurry, T. J.; Lauffer, R. B. *Chem. Rev.* **1999**, *99*, 2293−2352.
(3) Gries, H. *Top. Curr. Chem.* **2002**, *221*, 1−24.
(4) Weinmann, H. J.; Ebert, W.; Misselwitz, B.; Schmitt-Willich, H. *Eur. J. Radiol.* **2003**, *46*, 33−44.
(5) Weissleder, R.; Mahmood, U. *Radiology* **2001**, *219*, 316−333.
(6) Sipkins, D. A.; Cheresh, D. A.; Kazemi, M. R.; Nevin, L. M.; Bednarski, M. D.; Li, K. C. *Nat. Med.* **1998**, *4*, 623−626.

10.1021/ic049559g CCC: $27.50
Published on Web 09/03/2004

present in blood clots. Other work has focused on so-called "smart" contrast agents[8] that are sensitive to pH,[9−11] oxygen tension,[12,13] ions,[14,15] or enzymes.[16−18]

All of these compounds employ paramagnetic metal ions, M, and most function by shortening the T_1 of solvent water protons. The ability of a complex to enhance the relaxation rate of the solvent is termed relaxivity, and denoted r_1, eq 1

$$r_1 = \frac{\Delta 1/T_1}{[\mathrm{M}]} \tag{1}$$

and has units of $mM^{-1}\ s^{-1}$, where $\Delta 1/T_1$ is the change in relaxation rate of the solvent after addition of contrast agent of metal concentration [M]. High relaxivity means that the contrast agent can be detected at lower concentrations and may allow the imaging of low concentration molecular targets.

The relaxation mechanism is dipolar and depends on the ion-nuclear distance to the inverse 6th power ($1/r^6_{MH}$). Metal ions with a large spin number, S, are preferred, provided that electronic relaxation is slow. Complexes of gadolinium(III), high spin iron(III), and high spin manganese(II) have been used as relaxation agents.[19] The complex should have at least one site for water coordination and should undergo fast water exchange with the solvent. Perhaps the most important parameter that influences relaxivity is the rate of rotational diffusion. As rotational diffusion is slowed, the metal complex fluctuates at a frequency closer to the proton Larmor frequency and relaxation efficiency can be improved markedly. A particularly useful way to slow rotational rates is to incorporate a targeting functionality capable of binding the complex to a macromolecule.[20] This is dubbed the RIME effect (receptor induced magnetization enhancement), wherein binding to a target protein provides contrast not only by increasing the concentration of metal complex but also by increasing the relaxivity of the metal complex when targeted.[21] One example of this is MS-325, a derivative of the gadolinium complex of DTPA where the DTPA ligand was modified to bind noncovalently to serum albumin.[20] Serum albumin binding targets MS-325 to the blood vessels and causes a large increase in relaxivity. Once rotational diffusion is slowed, other correlation times (e.g., water residency time, electronic relaxation time) can limit relaxivity.

To date, most contrast agents are based on gadolinium(III). With seven unpaired electrons and relatively slow electronic relaxation, Gd(III) represents a particularly good choice for relaxation enhancement. Moreover, several stable complexes are known in which there is at least one site to coordinate an exchangeable water.[2] Although Gd(III) species are effective, it is beneficial to consider alternatives which may provide improved relaxivity. Other approaches have included superparamagnetic assemblies of iron oxide particles,[22,23] polymeric conjugates of gadolinium chelates,[24,25] and single chelates of other paramagnetic species.[26] This paper focuses on the possibility of using a manganese(II) complex as a high relaxivity agent.

Manganese(II) has five unpaired electrons and has long been used as a relaxation agent. Early research in MR imaging employed the use of $MnCl_2$ in dogs[27] and rats,[28] as well as in vitro systems involving this compounds' effect in human blood.[29] $MnCl_2$ is the active component of Lumenhance, a commercial contrast agent used for gastrointestinal imaging.[30] The liver imaging agent Mn-dipyridoxyldiphosphate $[Mn(DPDP)]^{4-}$, Telsascan has been studied extensively[31−35] and is the only Mn(II) complex approved for intravenous injection clinically. In his seminal review,

(7) Flacke, S.; Fischer, S.; Scott, M. J.; Fuhrhop, R. J.; Allen, J. S.; McLean, M.; Winter, P.; Sicard, G. A.; Gaffney, P. J.; Wickline, S. A.; Lanza, G. M. *Circulation* **2001**, *104*, 1280−1285.
(8) Lowe, M. P. *Aust. J. Chem.* **2002**, *55*, 551−556.
(9) Aime, S.; Barge, A.; Castelli, D. D.; Fedeli, F.; Mortillaro, A.; Nielsen, F. U.; Terreno, E. *Magn. Reson. Med.* **2002**, *47*, 639−648.
(10) Lowe, M. P.; Parker, D.; Reany, O.; Aime, S.; Botta, M.; Castellano, G.; Gianolio, E.; Pagliarin, R. *J. Am. Chem. Soc.* **2001**, *123*, 7601−7609.
(11) Zhang, S.; Wu, K.; Sherry, A. D. *Angew. Chem., Int. Ed. Engl.* **1999**, *38*, 3192−3194.
(12) Burai, L.; Toth, E.; Seibig, S.; Scopelliti, R.; Merbach, A. E. *Chem. Eur. J.* **2000**, *6*, 3761−3770.
(13) Aime, S.; Botta, M.; Gianolio, E.; Terreno, E. *Angew. Chem., Int. Ed. Engl.* **2000**, *39*, 747−750.
(14) Li, W.-h.; Fraser, S. E.; Meade, T. J. *J. Am. Chem. Soc.* **1999**, *121*, 1413−1414.
(15) Li, W.-h.; Parigi, G.; Fragai, M.; Luchinat, C.; Meade, T. J. *Inorg. Chem.* **2002**, *41*, 4018−4024.
(16) Louie, A. Y.; Huber, M. M.; Ahrens, E. T.; Rothbacher, U.; Moats, R.; Jacobs, R. E.; Fraser, S. E.; Meade, T. J. *Nature Biotechnol.* **2000**, *18*, 321−325.
(17) Moats, R. A.; Fraser, S. E.; Meade, T. J. *Angew. Chem., Int. Ed. Engl.* **1997**, *36*, 726−728.
(18) Nivorozhkin, A. L.; Kolodziej, A. F.; Caravan, P.; Greenfield, M. T.; Lauffer, R. B.; McMurry, T. J. *Angew. Chem., Int. Ed. Engl.* **2001**, *40*, 2903−2906.
(19) Lauffer, R. B. *Chem. Rev.* **1987**, *87*, 901−927.
(20) Caravan, P.; Cloutier, N. J.; Greenfield, M. T.; McDermid, S. A.; Dunham, S. U.; Bulte, J. W.; Amedio, J. C., Jr.; Looby, R. J.; Supkowski, R. M.; Horrocks, W. D., Jr.; McMurry, T. J.; Lauffer, R. B. *J. Am. Chem. Soc.* **2002**, *124*, 3152−3162.
(21) Lauffer, R. B. *Magn. Reson. Med.* **1991**, *22*, 339.
(22) Johansson, L. O.; Nolan, M. M.; Taniuchi, M.; Fischer, S. E.; Wickline, S. A.; Lorenz, C. H. *J. Cardiovasc. Magn. Reson.* **1998**, *1*, 139−143.
(23) Kellar, K. E.; Fujii, D. K.; Gunther, W. H. H.; Briley-Saebo, K.; Spiller, M.; Koenig, S. H. *Magn. Reson. Mater. Phys. Biol. Med.* **1999**, *8*, 207−213.
(24) Schmiedl, U.; Ogan, M.; Paajanen, H.; Marotti, M.; Crooks, L. E.; Brito, A. C.; Brasch, R. C. *Radiology* **1987**, *162*, 205−210.
(25) Schuhmann-Giampieri, G.; Schmitt-Willich, H.; Frenzel, T.; Press: W. R.; Weinmann, H. J. *Invest. Radiol.* **1991**, *26*, 969−974.
(26) Schwert, D. D.; Davies, J. A.; Richardson, N. *Top. Cur. Chem.* **2002**, *221*, 165−199.
(27) Lauterbur, P. C.; Mendoca-Dias, M. H.; Rudin, A. M. In *Front. Biol. Energetics*; Dutton, P. L., Leigh, L. S., Scarpa, A., Eds.; Academic: New York, 1978; Vol. 1, p 752.
(28) Mamourian, A. C.; Burnett, K. R.; Goldstein, E. J.; Wolf, G. L.; Kressel, H. Y.; Baum, S. *Physiol. Chem. Phys. Med. NMR* **1984**, *16*, 123−128.
(29) Kang, Y. S.; Gore, J. C.; Armitage, I. M. *Magn. Reson. Med.* **1984**, *1*, 396−409.
(30) Small, W. C.; DeSimone-Macchi, D.; Parker, J. R.; Sukerkar, A.; Hahn, P. F.; Rubin, D. L.; Zelch, J. V.; Kuhlman, J. E.; Outwater, E. K.; Weinreb, J. C.; Brown, J. J.; de Lange, E. E.; Woodward, P. J.; Arildsen, R.; Foster, G. S.; Runge, V. M.; Aisen, A. M.; Muroff, L. R.; Thoeni, R. F.; Parisky, Y. R.; Tanenbaum, L. N.; Totterman, S.; Herfkens, R. J.; Knudsen, J.; Bernardino, M. E. *J. Magn. Reson. Imaging* **1999**, *10*, 15−24.
(31) Rocklage, S. M.; Cacheris, W. P.; Quay, S. C.; Hahn, F. E.; Raymond, K. N. *Inorg. Chem.* **1989**, *28*, 477−485.
(32) Elizondo, G.; Fretz, C. J.; Stark, D. D.; Rocklage, S. M.; Quay, S. C.; Worah, D.; Tsang, Y. M.; Chen, M. C.; Ferrucci, J. T. *Radiology* **1989**, *178*, 73−78.
(33) Pomeroy, O. H.; Wendland, M.; Wagner, S.; Derugin, N.; Holt, W. W.; Rocklage, S. M.; Quay, S.; Higgins, C. B. *Invest. Radiol.* **1989**, *24*, 531−536.

Chart 1

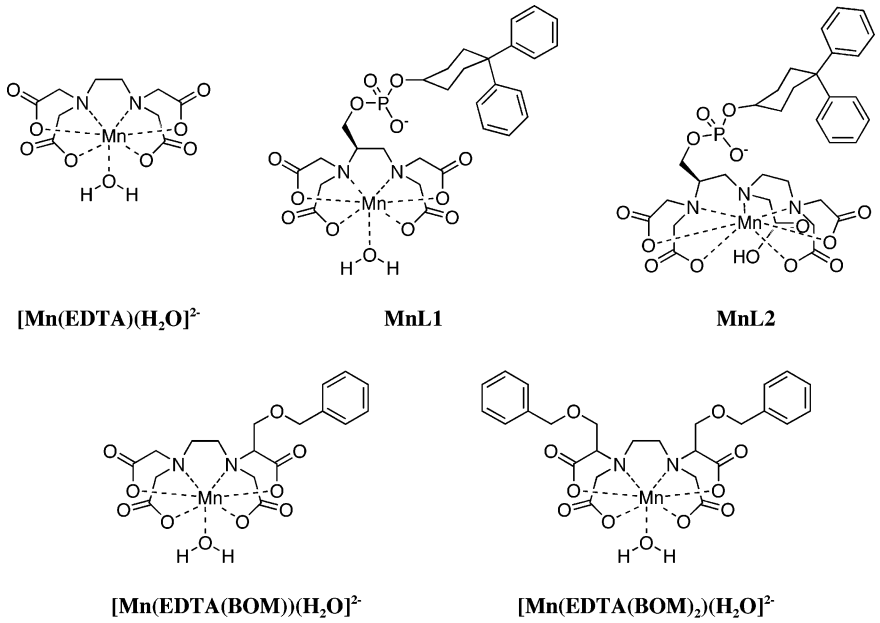

Lauffer[19] tabulated relaxivities for Mn(II) bound to proteins and pointed out that extremely large relaxivities (e.g., 275 mM^{-1} s^{-1} for Mn(II)-pyruvate kinase; 96 mM^{-1} s^{-1} for Mn(II)-concanavlin A) could be obtained for slow tumbling Mn(II) compounds. However, there is evidence suggesting that some manganese-based complexes are unstable in vivo,[36] which may limit their efficacy as contrast agents and may also cause unwanted release of free Mn(II) ion into the blood. Because of the high doses used in MRI, the stability of the metal complex has always been a large concern.

Previous work on $[Mn(EDTA)(H_2O)]^{2-}$ suggested that this complex may be a good core on which to synthesize a contrast agent. The sodium salt of the manganese EDTA complex is very well tolerated: LD_{50} is 7.0 mmol/kg in rats following intravenous injection compared with an LD_{50} of 0.22 mmol/kg for $MnCl_2$.[37] The EDTA complex is known to be 7-coordinate in the solid state,[38] and ^{17}O NMR studies are consistent with one coordinated water ($q = 1$) being present in aqueous solution.[39,40] In addition to possessing the critical exchangeable water, the water exchange rate[39] is close to an optimum value for a contrast agent (6.1×10^8 s^{-1} at 37 °C). It was also reasoned that the shorter $Mn-H_{water}$ distance would increase relaxivity and compensate for the lower spin number of Mn(II) ($S = 5/2$ for Mn(II), $S = 7/2$ for Gd(III)) when comparing relaxivity between Mn(II) and Gd(III) complexes. The relaxivities of the $q = 1$ complexes $[Mn(EDTA)(H_2O)]^{2-}$ and $[Gd(DTPA)(H_2O)]^{2-}$ are similar (2.9 and 4.1 mM^{-1} s^{-1}, respectively at 20 MHz, 35 °C).[41] The increased relaxivity of the Gd(III) complex may be due to its larger size and slower tumbling rate.

Decreasing the tumbling rate of Mn(II) complexes is known to have a positive influence on relaxivity. Early on, Lauffer et al.[42] showed that EDTA dianhydride could be reacted with the lysine residues of either bovine serum albumin or immunoglobulin G. The Mn(II) complex of the covalently protein bound EDTA-monoamide exhibited a marked increase in relaxivity ($r_1 = 26$ mM^{-1} s^{-1}) compared with $[Mn(EDTA)(H_2O)]^{2-}$. The presence of the inner sphere water was also critical: covalently linked Mn(DTPA-BSA) with $q = 0$ had a relaxivity of 3.4 $mM^{-1}s^{-1}$. Recently, Aime and colleagues reported Mn(II) complexes of EDTA derivatized with one or two benzyloxymethyl substituents (Chart 1).[43] These substituents are known to promote a noncovalent binding interaction with human serum albumin (HSA).[44,45] The HSA adducts of the manganese complexes had relaxivities of up to 10 times higher than the relaxivity in the absence of HSA.

(34) Tirkkonen, B.; Aukrust, A.; Couture, E.; Grace, D.; Haile, Y.; Holm, K. M.; Hope, H.; Larsen, A.; Lunde, H. S.; Sjogren, C. E. *Acta Radiol.* **1997**, *38*, 780−789.
(35) Brurok, H.; Skoglund, T.; Berg, K.; Skarra, S.; Karlsson, J. O. G.; Jynge, P. *NMR Biomed.* **1999**, *12*, 364−372.
(36) Gallez, B.; Baudelet, C.; Adline, J.; Geurts, M.; Delzenne, N. *Chem. Res. Toxicol.* **1997**, *10*, 360−363.
(37) Wolf, G. L.; Burnett, K. R.; Goldstein, E. J.; Joseph, P. M. In *Magnetic Resonance Annual 1985*; Kressel, H., Ed.; Raven: New York, 1985; p 231.
(38) Richards, S.; Pedersen, B.; Silverton, J. V.; Hoard, J. L. *Inorg. Chem.* **1964**, *3*, 27−33.
(39) Zetter, M. S.; Grant, M. W.; Wood, E. J.; Dodgen, H. W.; Hunt, J. P. *Inorg. Chem.* **1972**, *11*, 2701−2706.
(40) Oakes, J.; Smith, E. G. *J. Chem. Soc., Faraday Trans. 2* **1981**, *77*, 299−308.
(41) Koenig, S. H.; Baglin, C.; Brown, R. D., III.; Brewer, C. F. *Magn. Reson. Med.* **1984**, *1*, 496−501.
(42) Lauffer, R. B.; Brady, T. J.; Brown, R. D., III.; Baglin, C.; Koenig, S. H. *Magn. Reson. Med.* **1986**, *3*, 541−548.
(43) Aime, S.; Anelli, P. L.; Botta, M.; Brocchetta, M.; Canton, S.; Fedeli, F.; Gianolio, E.; Terreno, E. *J. Biol. Inorg. Chem.* **2002**, *7*, 58−67.
(44) Aime, S.; Botta, M.; Fasano, M.; Crich, S. G.; Terreno, E. *J. Biol. Inorg. Chem.* **1996**, *1*, 312−319.
(45) Aime, S.; Chiaussa, M.; Digilio, G.; Gianolio, E.; Terreno, E. *J. Biol. Inorg. Chem.* **1999**, *4*, 766−774.

Building on the work described above, a new Mn(II) complex was designed, synthesized, and evaluated in vitro and in vivo with regard to its nuclear relaxation properties. The present work describes the synthesis and characterization of a complex incorporating an EDTA functionality coordinating Mn(II), along with one water molecule in the inner coordination sphere. A diphenylcyclohexyl moiety, the same as used in MS-325, was linked to the EDTA via a phosphodiester and this group is used to target serum albumin. The effect of a binding group is 2-fold. First, it provides a means for targeting blood vessels for positive contrast. Second, albumin binding greatly reduces the rotational rate of the complex which further increases relaxivity. Binding data of the complex with serum albumin (rabbit and human) are reported. The relaxivity as a function of magnetic field strength and temperature are also reported for the compound in buffer only, serum albumin, and plasma. The rate of water exchange was estimated by variable temperature ^{17}O NMR. An analogous albumin binding Mn(II) complex based on DTPA ($q = 0$) was prepared and used to estimate the relaxation enhancement due to the exchanging water molecule. Favorable in vitro data prompted in vivo studies: plasma elimination kinetics and ex vivo relaxivity were measured and the compound was used for blood vessel imaging in a rabbit model. The data suggest that such an agent could be a viable alternative to gadolinium-based MRI contrast agents.

Experimental Section

Materials and Physical Measurements. Human serum albumin (HSA), product number A-1653 (Fraction V Powder 96−99% albumin, containing fatty acids) and rabbit serum albumin (RSA) were purchased from Sigma Chemical Company (St. Louis, Mo.). Citrated human plasma was received from Red Cross, Danvers, Massachusetts. Citrated rabbit plasma was obtained after fractionation of whole citrated blood that was drawn from New Zealand white rabbits. Ultrafiltration units (UFC3LCC00, regenerated cellulose membrane of 5,000 Dalton nominal molecular weight cutoff) were obtained from Millipore Corporation; Bedford, MA. Cyanoethyl diisopropyl phosphoramidochloridate was purchased from Toronto Research Chemicals. Other reagents were supplied by Aldrich Chemical Co., Inc., and were used without further purification. NMR spectra of synthetic intermediates were obtained with a Varian Unity 300 spectrometer. All spectra were recorded in $CDCl_3$ solution at 25°C unless noted otherwise. ^1H NMR (300 MHz) and ^{13}C NMR (75 MHz) chemical shifts were referenced to residual solvent resonances (^1H $\delta = 7.26$ ppm and ^{13}C $\delta = 77.16$ ppm for $CDCl_3$, or as noted). ^{31}P NMR (121 MHz) chemical shifts were referenced to external H_3PO_4 in THF solution ($\delta = 0$ ppm). Elemental analyses were performed by Galbraith Laboratories (Knoxville, TN).

Synthesis of ligand. (R)-2,3-diaminopropan-1-ol bis hydrochloride (2) L-serinamide hydrochloride (**1**) (15.00 g, 107 mmol, 1.0 eq.) was suspended in methanol (500 mL) and Amberlite IR-440C strongly basic cation-exchange resin (~50 g) was added and the mixture was stirred slowly for 1 h. The resin was removed by filtration, and washed with several portions of methanol. Evaporation of methanol filtrate gave the free base as a white powder. The free base L-serinamide was suspended in THF (300 mL) and the mixture cooled to 0−5 °C on an ice bath. While stirring under argon, borane−THF complex (500 mL of 1 mmol/mL BH_3 complex, 5 eq.) was added dropwise via addition funnel while maintaining a temperature of 0−15 °C. The temperature was then increased to 65 °C and the solution stirred for 18 h. The solution was then cooled to 5 °C, and 5 M HCl (200 mL) was added very slowly, maintaining temperature at <20 °C. THF was removed by rotary evaporation. An additional portion of concentrated HCl (200 mL) was added and the solution warmed to 95 °C and stirred for 2 h. The solution was then reduced in volume by 75% by rotary evaporation, cooled to 0 °C, and filtered. An additional portion of concentrated HCl (100 mL) was added, and the mixture was allowed to stand at 0 °C for 1 h. The white precipitate was removed by filtration. The remaining solution was concentrated to a mixture of an oil and white solid by rotary evaporation. The mixture was triturated with several portions of ethanol affording **2** as a white powder (11.1 g, 64%). Anal. Calcd for $C_3H_{10}N_2O\cdot 2HCl$: C, 22.10; H, 7.42; N, 17.18; Cl, 43.49. Found: C, 22.24; H, 7.60; N, 17.09; Cl, 43.54. ^1H NMR (D_2O): δ 3.87 (m, 2H), 3.74 (m, 1H), 3.89 (m, 2H). ^{13}C NMR (DMSO-*d*6): δ 38.24, 50.51, 58.86.

(*R*)-{[2-(Bis-*tert*-butoxycarbonylmethyl-amino)-1-hydroxymethyl-ethyl]-*tert*-butoxycarbonylmethyl-amino}-acetic Acid *tert*-Butyl Ester (3). 2 (12.2 g, 75 mmol, 1 eq), diisopropylethylamine (157 mL, 900 mmol, 12 eq), and potassium iodide (24.9 g, 150 mmol, 2 eq) were dissolved in DMF (200 mL) and the solution warmed to 35 °C. *Tert*-butylbromoacetate (87.8 g, 450 mmol, 6.0 eq.) was added dropwise over 20 min. The solution was stirred for 1 h at 35 °C and cooled to room temperature. DMF was removed by rotary evaporation, and the residue was partitioned between 10% $NaHCO_3$ and ethyl acetate. The aqueous layer was extracted with three additional portions of ethyl acetate. Combined organic layers were then washed with brine, and dried over Na_2SO_4. Evaporation gave a dark brown oil that was purified by flash chromatography (SiO_2, hexanes/EtOAc 9:1 to 5:1 to 3:1). The desired product **3** was obtained as a light brown oil (33.7 g, 82%). Anal. Calcd for $C_{27}H_{50}N_2O_9\cdot H_2O$: C, 58.36; H, 9.25; N, 5.04. Found: C, 58.71; H, 9.25; N, 4.93. ES^+-MS: *m*/*z* 548 $[M+H]^+$. ^1H NMR: δ 1.44 (m, 36H), 2.50−2.65 (m, 1H), 2.79−3.04 (m, 2H), 3.38 (s, 4H), 3.45 (s, 4H), 3.48−3.74 (m, 2H), 4.2−4.6 (bs, 1H). ^{13}C NMR: δ 28.17, 53.71, 53.93, 56.46, 81.19, 170.53, 171.98.

(*R*)-({2-(Bis-*tert*-butoxycarbonylmethyl-amino)-3-[(2-cyanoethoxy)-diisopropylamino-phosphanyloxy]-propyl}-*tert*-butoxycarbonylmethyl-amino)-acetic Acid *tert*-Butyl Ester (4). 3 (29.8 g, 54.4 mmol, 1.0 eq.) and diisopropylethylamine (10.0 mL, 57.4 mmol, 1.05 eq.) were dissolved in CH_2Cl_2 (125 mL). A solution of cyanoethyldiisopropylphosphoramido chloridate (11.6 g, 49.0 mmol, 0.9 eq.) in 50 mL CH_2Cl_2 was added to the reaction mixture over 1 min. The solution was stirred for 30 min at room temperature. An additional portion of cyanoethyldiisopropylphosphoramido chloridate (1.3 g, 5.4 mmol, 0.1 eq.) was added, and the solution stirred for an additional 50 min. The solution was diluted with CH_2Cl_2 (250 mL) and washed with cold saturated $NaHCO_3$, and dried over Na_2SO_4. Evaporation gave an oil that was purified by flash chromatography (SiO_2, hexanes/EtOAc/triethylamine 90:10:0.1 to 80:20:0.1). The phosphoramidite **4** was obtained as a light brown oil (37.9 g). ^{31}P NMR: δ 141.50 (d). An impurity (^{31}P NMR: δ 140.00 (s)), approximately 20% of the ^{31}P signal, was not removed during the purification. The intermediate was used without further characterization.

(R)−({2-(Bis-*tert*-butoxycarbonylmethyl-amino)-1-[(4,4-diphenyl-cyclohexyloxy)-hydroxy-phosphoryloxymethyl]-ethyl}-*tert*-butoxycarbonylmethyl-amino)-acetic Acid *tert*-Butyl Ester (5). 4,4-Diphenylcyclohexanol[46] (13.5 g, 53.4 mmol, 1.05 eq.) and molecular sieves (15.0 g) were suspended in a solution of **4** (38.0

g, 50.9 mmol, 1.0 eq.) in acetonitrile (200 mL). A 3% solution of 1H-tetrazole in acetonitrile (3.7 g of 1H-tetrazole, 53.4 mmol, 1.05 eq) was added at once, and the suspension was stirred for 1 h. A 70% aqueous solution of *tert*-butylhydroperoxide (25 mL) was then added and most of the suspended solids dissolved. The mixture was stirred for 1 h. Molecular sieves were removed by filtration, and volatiles were then reduced in volume by 50% by rotary evaporation. The remaining residue was dissolved in 300 mL ethyl acetate, and the organic layer was washed with 10% $Na_2S_2O_3$, saturated $NaHCO_3$ and brine, and then dried over Na_2SO_4. The ethyl acetate was evaporated, and the residue was treated with a 3 M solution of ammonia in methanol (450 mL) and stirred for 6 h. The methanol was removed by rotary evaporation, and the crude **5** was purified by flash chromatography (SiO_2, MeOH:CH_2Cl_2:Et_3N 1:99:0 to 2:98:0 to 2:98:0.2 to 4:96:0.4 to 8:92:0.4) to give the desired triethylammonium salt of **5** as an oil (27.5 g, 58%). ES^+-MS: *m*/*z* 862 $[M+H]^+$. ^1H NMR: δ 1.21(t, 10H), 1.40 (m, 36H), 1.60−1.76 (m, 2H), 1.80−2.00 (m, 2H), 2.00−2.20 (m, 2H), 2.40−2.60 (m, 2H), 2.60−3.30 (m, 10H), 3.41 (s, 1H), 3.40−3.60 (m, 8H), 3.67 (s, 1H), 3.88−4.03 (m, 2H), 4.25−4.30 (m, 1H), 7.06−7.11 (m,2H), 7.17−7.29 (m, 8H). ^{13}C NMR: δ 8.68, 27.79, 29.54, 33.01, 45.19, 45.32, 53.57, 53.83, 55.92, 30.78, 40.58, 64.24, 72.46, 80.05, 80.26, 121.23, 125.16, 126.42, 126.87, 127.85, 127.93, 134.98, 146.80, 147.94, 170.55, 170.95. ^{13}P NMR: δ 4.46.

L1. Protected ligand **5** (22.8 g, 24.6 mmol) was dissolved in acetonitrile (200 mL), and concentrated hydrochloric acid (50 mL) was added at 0 °C over 5 min. The solution was stirred for 18 h. An additional portion of hydrochloric acid (20 mL) was added, and the solution was stirred an additional 1 h. The volume was reduced by approximately 75% by rotary evaporation. The residue was diluted with water (150 mL) and the pH was adjusted to ∼1.6 by the addition of sodium hydroxide. The white precipitate was collected by filtration and washed with H_2O (pH = 1.6), ether (50 mL), and ethyl acetate (50 mL). The monohydrate of **L1** was obtained as a white powder (12.7 g, 81%). Anal. Calcd for $C_{29}H_{37}N_2O_{12}P\cdot H_2O$: C, 53.21; H, 6.01; N, 4.28; P, 4.73. Found: C, 53.69; H, 6.12; N, 4.31; P, 4.39. ES^+-MS: *m*/*z* 637 $[M+H]^+$, 659 $[M+Na]^+$. IR (AMTIR cell, aqueous solution, pH = 6): 1611 (s, ν_{asym} CO_2^-), 1401 (s, ν_{sym} CO_2^-), 1323 (m), 1206 (m), 1074 (m), 1017 (m), 994 (m) cm^{-1}. ^1H NMR (D_2O + NaOD, pD = 13): δ 1.51−1.54 (m, 2H), 1.70−1.90 (m, 2H), 2.00−2.10 (m, 2H), 2.18 (d, 1H), 2.39−2.60 (m, 3H), 2.70−2.80 (m, 3H), 3.60−3.80 (m, 2H), 4.00−4.20 (m, 1H), 7.00−7.35 (m, 10H). ^{13}C NMR (CD_3OD): δ 31.06, 34.23, 46.74, 53.64, 55.35, 56.17, 59.55, 64.02, 75.80, 126.82, 128.04, 128.39, 129.41, 129.55, 148.64, 149.43, 171.00, 174.93. ^{31}P NMR: δ −2.99.

MnL1. Ligand **L1** (12.7 g, 19.5 mmol, 1.0 eq.) was dissolved in water (100 mL), and the pH was adjusted to ∼6 with dropwise addition of 1 M NaOH. Solid $MnCl_2\cdot 4H_2O$ (3.9 g, 19.5 mmol, 1.0 eq.) was added with stirring. The solution was stirred for 15 min while maintaining a pH of 6. The solution was lyophilized affording crude chelate. Inorganic impurities were removed by two sequential elutions through pre-packed and equilibrated C18 columns with a gradient of water to 1:1 ethanol:water and conductivity detection. Ethanol was removed by rotary evaporation, and the remaining aqueous solution was lyophilized to afford purified chelate **MnL1** as the tetrahydrate trisodium salt as a white solid (6.8 g, 45.1%). Anal. Calcd for $C_{29}H_{32}MnNa_3N_2O_{12}P\cdot 4H_2O$: C, 42.09; H, 4.87; N, 3.39; Mn, 6.63; Na, 8.33; P, 3.74. Found: C, 42.16; H, 5.50; N, 3.18; Mn, 6.48; Na, 8.37; P, 3.71. **MnL1** on a HPLC-MS with UV (220 nm) and +ESI detection (see Supporting Information for trace) with a gradient of 50 mM ammonium formate with 5% (9:1 ACN:50 mM ammonium formate) rising to 50% (9:1 ACN:50 mM ammonium formate) over 20 min (15.0 μL/min, Thermo-Keystone HyPurity C18, 0.5 × 150 mm, 5 μm) elutes at 14.38 min (97.1% total peak area at 220 nm, positive ion, *m*/*z* = 690 [M+4H]+). IR (AMTIR cell, aqueous solution, pH = 6): 1584 (s, ν_{asym} CO_2^-), 1413 (s, ν_{sym} CO_2^-), 1330 (m), 1200 (m), 1072 (m), 1022 (m), 993 (m) cm^{-1}.

MnL2. The ligand **L2** was prepared as described previously.[47] The manganese complex was prepared in solution and not isolated. The concentration of the ligand **L2** was determined by photometric tritration with $Gd(NO_3)_3$ as described previously.[20] To a 1.04 mL solution of **L2** (57.1 mM, 59.4 μmol) at pH 6.5 was added 11.2 mg of $MnCl_2\cdot 4H_2O$ (56.6 μmol), and the pH was adjusted to 6.5 by addition of 1 M NaOH. The solution was stirred for 30 min. The solution was analyzed by HPLC with UV and ESI detection using a gradient of 50 mM ammonium formate with 5% (9:1 ACN:50 mM ammonium formate) to 40% (9:1 ACN:50 mM ammonium formate) over 15 min (0.8 mL/min, Kromasil C4, 4.6 × 250 mm, 5 μm). L2 eluted at 11.5 min (3.0% total peak area at 220 nm, negative ion, *m*/*z* = 736 [M−H]-) and **MnL2** eluted at 12.5 min (97.0% of total peak area, negative ion, *m*/*z* = 789 [M+2H]-).

Ultrafiltration Measurements of Binding. Solutions containing 0.1 mM Mn chelate and serum albumin (4.5% w/v) were prepared by mixing appropriate volumes of **MnL1** or **MnL2** stock solution, 6% serum albumin (RSA or HSA), and PBS. Plasma solutions were prepared by first making a stock solution by adding solid **MnL1** or **MnL2** to plasma (human or rabbit); the stock was diluted to the appropriate Mn solution by the addition of plasma. Two aliquots (400 μL) of each of these samples were placed in 5 kDa ultrafiltration units. Two additional 25 μL aliquots were analyzed by ICP-MS to determine the total Mn concentration. The samples were incubated at 37 °C for 10 min and then centrifuged at 5800 g for 3.5 min. The filtrates (∼30 μL) from these ultrafiltration units were used to determine the free concentration of complex in each of the samples by ICP-MS.

Relaxivity. Relaxivities were determined at 20 MHz (0.47 T) and 60 MHz (1.4 T) using Bruker Minispecs, NMS 120 and mq60, respectively to determine T_1. T_1 was measured with an inversion recovery pulse sequence and all samples were measured at 37 °C. Relaxivity was obtained from the slope of a plot of $1/T_1$ versus concentration for 0, 20, 40, and 60 μM Mn samples in 660 μM HSA, 660 μM RSA, human plasma, or rabbit plasma. Relaxivities in HEPES (pH 7.4) buffer were determined using solutions of 0, 100, 150, and 200 μM Mn. The ^1H NMRD profiles (5, 15, 25, and 35 °C) were recorded on a field cycling relaxometer at NY Medical College over the frequency range 0.01−50 MHz. A total of 22 data point dispersions were recorded at each temperature. Manganese concentration was 70 μM and the HSA or RSA was 660 μM. Relaxivity was computed by subtracting the relaxation rate of the medium (HSA or RSA in HEPES) from the relaxation rate of the Mn solution at each field strength and dividing the difference by the manganese concentration in millimolar. All solutions were assayed for manganese concentration by ICP-MS.

^{17}O NMR. $H_2{}^{17}O$ transverse relaxation rates were determined for a PBS buffer solution in the presence and absence of 1.10 mmolal **MnL1** as a function of temperature (0−80 °C) on a Varian Unity 300 NMR operating at 40.6 MHz. Probe temperatures were determined from ethylene glycol or methanol chemical shift

(46) Amedio, J. C., Jr.; Bernard, P. J.; Fountain, M.; Van Wagenen, G., Jr. *Synth. Commun.* **1998**, *28*, 3895−3906.

(47) McMurry, T. J.; Parmelee, D. J.; Sajiki, H.; Scott, D. M.; Ouellet, H. S.; Walovitch, R. C.; Tyeklar, Z.; Dumas, S.; Bernard, P.; Nadler, S.; Midelfort, K.; Greenfield, M.; Troughton, J.; Lauffer, R. B. *J. Med. Chem.* **2002**, *45*, 3465−3474.

Scheme 1

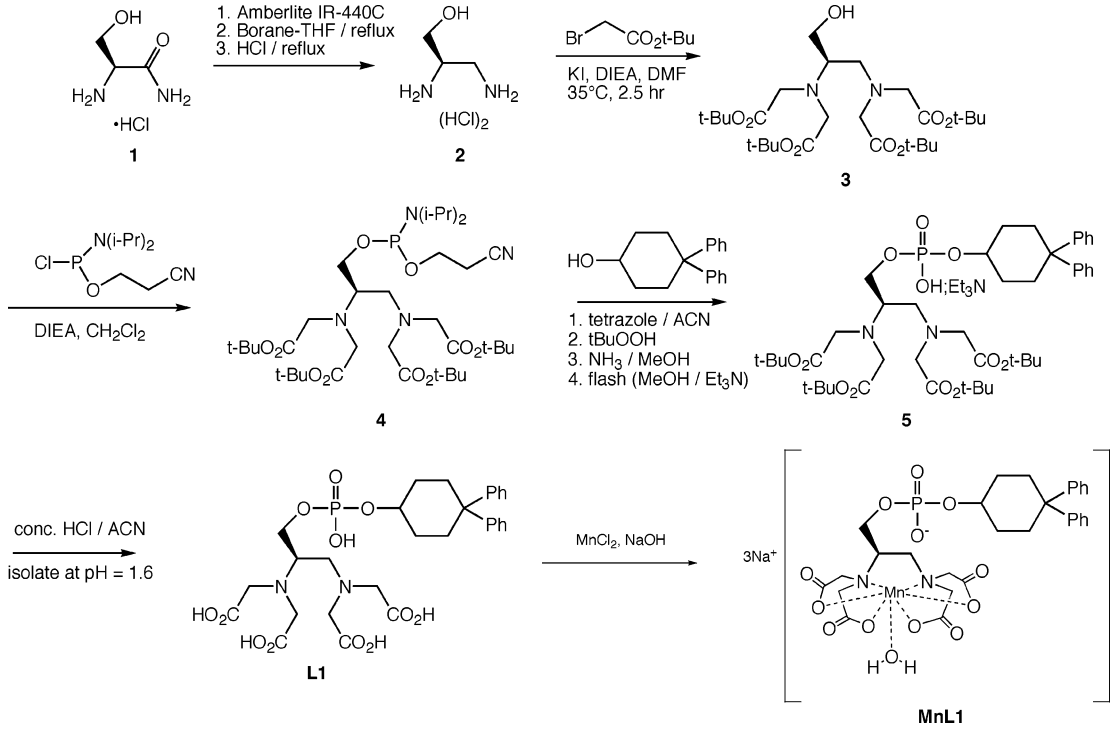

calibration curves. T_2 was determined by a CPMG pulse sequence. Measurements were repeated after heating to ensure reproducibility.

Rabbit Pharmacokinetics. A conscious rabbit weighing approximately 2 kg was injected via the marginal ear vein with **MnL1** (30 μmol/kg) and venous blood samples (1 mL) were withdrawn at −5, 1, 3, 6, 9, 12, 15, 20, 30, 45, and 60 min postinjection. Blood was collected in sodium citrate tubes and the tubes were centrifuged 10 min at 3000 rpm to isolate the plasma (∼0.5 mL). The plasma samples were assayed for manganese using ICP-MS and the proton T_1 of each plasma sample was determined at 60 MHz as described above.

Animal Surgical Protocol. All animal procedures were approved and were performed in accordance with the EPIX Medical animal care committee. Adult New Zealand white rabbits (F, 2−3 kg, Harlan Indianapolis, IN) were sedated with ketamine 8 mg/kg, i.m. and xylazine 2 mg/kg, i.m. and anesthetized with pentobarbital 20 mg/kg, i.v. Catheters were placed in the marginal ear vein and artery for agent administration and blood withdrawals, respectively. A lateral mid-line incision was made in the ventral neck region and the carotid artery and jugular vein were isolated and circumscribed with suture. To induce an arterial thrombus, a 5 mm section of the carotid artery was isolated and a fixed stenosis placed distally using an 18 gauge needle and 4−0 silk suture. The arterial section was occluded and endothelial damage induced by crushing the vessel using a hemostat. Approximately 3 min later, flow was reestablished. A venous thrombus was formed by occluding a 5 mm section of the jugular vein and introducing a thrombin-soaked silk suture into the vessel. In addition, 100 μL of a solution comprised of whole blood, thrombin 1.9 IU, and $CaCl_2$ 58 mM was injected into the occluded segment. Three minutes later, flow was reestablished. The surgical area was sutured closed and approximately 20 mL of saline was placed in the incision site to remove air. After the thrombi had aged for over an hour, **MnL1** (10 μmol/kg), was administered for anatomical verification.

Imaging. Imaging studies were performed in a GE CVI 1.5 T scanner. The imaging sequence was a 3D gradient recalled echo with rf spoiling using a circular, linear RF coil with a 3 in. diameter. Chemical fat saturation was applied. In addition, superior and inferior spatial saturation bands were used to null flowing blood. Scan parameters: 256 × 256 pixels; NEX = 1; Phase FOV = 0.75; TR = 39 ms; TE = 3.1 ms; BW = 16 kHz (61 Hz/pixel); FOV = 8 cm; slice thickness = 0.8 mm interpolated to 0.4 mm; partitions per slab = 64; total scan time = 8:02 min. Contrast-to-noise ratio (CNR) is defined as (blood SI − muscle SI)/background SI.

Results and Discussion

The ligand, **L1** (Chart 1), is the EDTA analogue of the ligand, **L2**, used in the synthesis of the gadolinium based contrast agent, MS-325.[20,48] It was reasoned that the EDTA would provide a stable manganese(II) complex with one coordinated water (vide supra) and that the diphenylcyclohexyl moiety would promote binding to serum albumin.[20] The manganese(II) complex of **L2** could serve as an albumin binding control complex with no inner sphere water, as it is known that Mn-DTPA complexes are coordinatively saturated by the DTPA ligand.[41,49]

The synthesis of **MnL1** from L-serinamide hydrochloride is described in Scheme 1. L-Serinamide hydrochloride **1** was first neutralized with a strongly basic cation-exchange resin. The free L-serinamide was then reduced to the corresponding diamine **2** with borane-THF. Alkylation of **2** with *tert*-butyl-2-bromoacetate under conditions reported previously[50] gave the protected hydroxymethyl-EDTA **3** in good yield after

(48) Lauffer, R. B.; Parmelee, D. J.; Dunham, S. U.; Ouellet, H. S.; Dolan, R. P.; Witte, S.; McMurry, T. J.; Walovitch, R. C. *Radiology* **1998**, *207*, 529−538.
(49) Oakes, J.; Van Kralingen, C. G. *J. Chem. Soc., Dalton Trans.* **1984**, 1133−1137.
(50) Amedio, J. C., Jr.; Bernard, P. J.; Fountain, M.; Van Wagenen, G., Jr. *Synth. Commun.* **1999**, *29*, 2377−2391.

Table 1. Relaxivity of **MnL1** and **MnL2** in Various Media, 20 MHz, 37 °C, pH 7.4 Error in Relaxivity Estimated at ±5%

medium	**MnL1** r_1 ($mM^{-1}s^{-1}$)	**MnL2** r_1 ($mM^{-1}s^{-1}$)
HEPES buffer	5.8	3.0
rabbit plasma	51	7.7
rabbit serum albumin	47	7.0
human plasma	46	5.3
human serum albumin	48	4.6

flash chromatography. The incorporation of the albumin binding group via phosphodiester linkage proceeded by converting **3** to the cyanoethyldiisopropyl phosphoramidite **4** and subsequent tetrazole catalyzed displacement of diisopropylamine with 4,4-diphenylcyclohexanol.[46] The resulting phosphite was oxidized to the corresponding phosphotriester with *tert*-butylhydroperoxide. Following cleavage of the cyanoethyl protection with ammonia and purification by flash chromatography with triethylamine in the eluant, the protected ligand **5** was obtained in moderate yield as the triethylammonium salt. After deprotection with hydrochloric acid, the ligand **L1** was isolated from the reaction mixture in high purity by precipitation at pH 1.6. The manganese complex **MnL1** was prepared by reaction of **L1** with a stoichiometric equivalent of $MnCl_2$ at pH 6 followed by removal of inorganic impurities by reverse-phase chromatography. The pure chelate was isolated by lyophilization as the trisodium salt in moderate yield and gave satisfactory elemental analysis with the exception of hydrogen which was too high. However the other 5 elements analyzed were within 0.2 percentage units of the expected values. HPLC-MS analysis (Supporting Information) of **MnL1** under neutral conditions (pH 6.8) gave an estimated purity of 97.1%. Electrospray MS showed the parent ion of the complex. The IR spectrum was similar to that of **L1**. The carboxylate stretching frequencies shifted upon complexation consistent with carboxylate coordination of the Mn(II) ion.

The relaxivities of **MnL1** were determined initially in HEPES buffer and in rabbit plasma, Table 1. A dramatic 9-fold increase in relaxivity was observed when going from buffer only to plasma. The relaxivity in rabbit plasma is considerably higher than that of commercial MRI contrast agents (14-fold) and higher than that of most high relaxivity gadolinium complexes. Similar high relaxivity values were obtained in human plasma. It was hypothesized that the increase in relaxivity upon going from buffer only to plasma was a result of (1) an increase in the rotational correlation time of the molecule because of binding to the slow tumbling plasma protein, serum albumin, and (2) a rapidly exchanging inner sphere water molecule that transmitted an efficient relaxation mechanism from the inner-coordination sphere to the bulk solvent.

To test this hypothesis, the relaxivity of **MnL1** in physiological concentrations of rabbit or human serum albumin (RSA or HSA, respectively) was determined, and found to be similar to the value obtained for the corresponding plasma. In addition, the binding of **MnL1** to plasma proteins or serum albumin was determined by ultrafiltration with a 5 kDa molecular weight cutoff, Table 2. The binding study demonstrates that **MnL1** is greater than 90% bound to protein at 0.1 mM manganese concentration. The similarity in relaxivity between serum albumin and plasma along with the similarity in fraction bound between serum albumin and plasma suggest that **MnL1** is bound predominantly to serum albumin in plasma.

Table 2. Binding of 0.1 MM **MnL1** and **MnL2** to Plasma Proteins and Serum Albumin (4.5% w/v) at pH 7.4, 37 °C[a]

medium	**MnL1** % bound	**MnL2** % bound
rabbit plasma	96	74
rabbit serum albumin	89	81
human plasma	93	70
human serum albumin	98	92

[a] Relative error in percent bound estimated at 2%.

These results can be compared with what was observed for MS-325 (the Gd(III) complex of **L2**).[20] Under the same conditions MS-325 was 88% bound to HSA which is somewhat lower than that of **MnL1** with HSA (98%). It is not clear why the HSA affinity is higher for **MnL1** than MS-325. Both compounds have the same overall charge (−3); the smaller EDTA derived **MnL1** may be preferred based on size. To compare the relaxivities of **MnL1** and MS-325 it is useful to consider the so-called bound relaxivity, r_1^{bd}. The bound relaxivity is calculated from a knowledge of the free and bound fractions and the relaxivity of the free fraction. Using the observed relaxivities in Table 1 along with the fraction bound in Table 2, one calculates a bound relaxivity of 49 mM^{-1} s^{-1} for **MnL1** bound to HSA compared with a value of 51 mM^{-1} s^{-1} for MS-325 bound to HSA.[20] The similar relaxivities suggest that the effect of the smaller spin quantum number, *S*, for Mn(II) vs Gd(III) is offset by a shorter Mn−H distance

It is expected that **MnL1** contains a coordinated inner sphere water molecule. The EDTA complex of Mn(II) is known to be 7-coordinate with a water bound to the metal ion.[38,39,41] Both $[Mn(EDTA)(H_2O)]^{2-}$ and the Mn-EDTA derivatives reported by Aime et al.[43] gave relaxivities consistent with the complexes being $q = 1$. To assess the effect of the inner sphere water molecule the potentially octadentate DTPA derivative, **L2** (Chart 1) was used to form a $q = 0$ Mn(II) complex, **MnL2**. The DTPA complex of Mn(II) is known to contain no inner sphere water.[41,49]

The relaxivity of **MnL2** was about half that of **MnL1** in HEPES, which is consistent with it forming a $q = 0$ complex. **MnL2** also has reasonable affinity for serum albumins, Table 2, although the affinity is somewhat lower than for the EDTA-based ligand. The lower affinity of **MnL2** for albumins compared with that of **MnL1** may be a result of the increased negative charge on **MnL2.** The relaxivity of **MnL2** increases when bound to albumin (Table 1). Although the increase is not as marked as with **MnL1**, the relaxivity is 50−150% higher in plasma or albumin solution. Similar increases have been reported for other $q = 0$ complexes bound to albumin. [20,42,51,52]

(51) Aime, S.; Batsanov, A. S.; Botta, M.; Howard, J. A. K.; Parker, D.; Senanayake, K.; Williams, G. *Inorg. Chem.* **1994**, *33*, 4696−4706.
(52) Jenkins, B. G.; Armstrong, E.; Lauffer, R. B. *Magn. Reson. Med.* **1991**, *17*, 164−178.

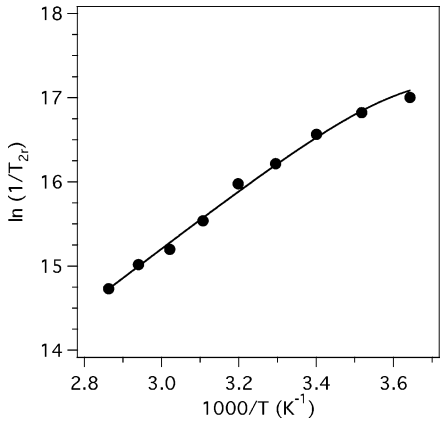

Figure 1. Reduced transverse ^{17}O relaxation rates ($1/T_{2r}$) for water in the presence of **MnL1** as a function of reciprocal temperature.

Table 3. Water Exchange and Electronic Relaxation Parameters for **MnL1** in HEPES Buffer (pH 7.4) in the Absence of Albumin (7.05 T)[a]

k_{ex}^{298} (s^{-1})	τ_m^{310} (ns)	$\Delta H^{\ddagger}$ (kJ mol^{-1})	T_{1e} (ns)	co-ligand
$2.3 \pm 0.9 \times 10^8$	2.1−5.0	23−27	> 4	**L1**
4.4×10^8	1.4	32		EDTA[39]
0.93×10^8	6.7	43.1		EDTA(BOM) [43]
1.3×10^8	5.2	38.4		$EDTA(BOM)_2$[43]

[a] The range given corresponds to a fixed T_{1e} of either 4 or 2000 ns. Water exchange rates at 25 °C (298 K) and residency times at 37 °C (310 K) for $[Mn(EDTA)(H_2O)]^{2-}$ and two EDTA derivatives are listed for comparison.

Qualitatively, the high relaxivity can be explained by the rapid exchange of an inner sphere water molecule from a slow tumbling metal complex. To better understand this process and to determine whether it would be possible to further optimize relaxivity with a manganese(II) complex, variable temperature and variable field relaxation studies were carried out.

The water exchange rate of **MnL1** was determined using the temperature dependence of the ^{17}O transverse relaxation rate. Based on earlier work,[39,53] the hyperfine coupling constant, $A/\hbar$, between Mn(II) and the water oxygen was set to 3.79×10^7 rad/s. The reduced relaxation rates (the paramagnetic relaxation rate due to the bound water, see the Supporting Information for more details) are plotted versus reciprocal temperature in Figure 1. In the fast exchange regime, nuclear transverse relaxation is governed by a scalar mechanism with a correlation time that has contributions from the water exchange rate ($k_{ex} = 1/\tau_m$) and the electronic relaxation rate ($1/T_{1e}$). At the field strength used (7 T), the electronic relaxation rate of Mn(II) is slower than the water exchange rate, and it was not possible to get a good estimate of the electronic relaxation rate. An upper bound on the electronic relaxation rate was determined by increasing the rate arbitrarily until the quality of the fit deteriorated. In Table 3, the parameters derived from the fitting are listed as correlation times. The activation enthalpy corresponds to the Eyring equation (see the Supporting Information for further details). The range of values for τ_m and $\Delta H^{\ddagger}$ come from fixing T_{1e} at short (4 ns) and long (2000 ns) times. The values in Table 3 demonstrate that τ_m and its temperature dependence are rather independent of T_{1e}.

The value of τ_m determined here is very similar to that reported by Zettler et al.[39] for $[Mn(EDTA)(H_2O)]^{2-}$ and for the Mn(II) complexes of the EDTA derivatives reported by Aime et al.[43] In all instances, τ_m at 37 °C is between 2 and 7 ns. There is little, if any, effect on water exchange by modifying the EDTA ligand either on the ethylenediamine backbone (this work) or on one of the acetate arms.[43] The short value of τ_m suggests that proton relaxivity should not be limited by slow water exchange, as has been observed with some gadolinium-based contrast agents.

Proton relaxation rates ($1/T_1$) were determined over the frequency range 0.01−50 MHz for **MnL1** in the presence and absence of serum albumin. It is known that compounds with no water in the inner-coordination sphere may still exhibit significant relaxivity. To estimate the contribution to relaxivity from the inner sphere water molecule, the NMRD profile of **MnL2** was determined in the same medium and at the same temperature. In total, 16 NMRD profiles were determined: **MnL1** (0.1 mM) in 4.5% HSA at 5, 15, 25, 35 °C; **MnL1** (0.1 mM) in 4.5% RSA at 5, 15, 25, 35 °C; **MnL2** (0.1 mM) in 4.5% HSA at 5, 15, 25, 35 °C; **MnL2** (0.1 mM) in 4.5% RSA at 5, 15, 25, 35 °C. These observed relaxivities are given in Tables S1 − S4 in Supporting Information. Observed relaxivity (r_1^{obs}) can be factored into inner sphere (IS), second sphere (SS), and outer-sphere (OS) components. It is difficult to account for how much these 2nd sphere waters contribute to the observed relaxivity because the number of water molecules in the 2nd coordination sphere, the ion-nuclear distance for these waters, and the lifetimes of these waters are unknown. Therefore, it was assumed that the relaxivity of **MnL2** is similar to the second and outer-sphere relaxivity of **MnL1**. By subtracting the relaxivity of **MnL2** from **MnL1**, an estimate of the inner sphere relaxivity for **MnL1** is obtained, eqs 2 and 3. This is shown in Figure 2 where the NMRD profiles of the observed relaxivities of **MnL1** and **MnL2** in RSA at 35 °C are plotted

$$r_1^{obs} = r_1^{IS} + r_1^{SS} + r_1^{OS} \quad (2)$$

$$r_1^{IS}(MnL1) \approx r_1^{obs}(MnL1) - r_1^{obs}(MnL2) \quad (3)$$

Using the observed relaxivity of **MnL2** as an estimate of the 2nd sphere and outer-sphere relaxivity of **MnL1** is an approximation. The alternative would be to add additional parameters in the curve fitting which would only increase the ambiguity of the resultant determined parameters.

EPR studies indicated that the static zero-field splitting (ZFS) for **MnL1** was quite large ($D \sim 900$ G).[54] In the interpretation of the nuclear relaxation rate data, only those data points in the high field limit were considered (only where $E_{Zeeman} > E_{ZFS}$, i.e., data at 8 MHz and higher frequencies). In this high field limit ($\mathbf{B}_0 \geq 0.2$ T), the data can be modeled with simple analytical expressions (the Solomon-Bloembergen-Morgan, SBM, equations). To treat

(53) Ducommun, Y.; Newman, K. E.; Merbach, A. E. *Inorg. Chem.* **1980**, *19*, 3696−3703.

(54) Raitsimring, A. M.; Caravan, P. Manuscript in preparation.

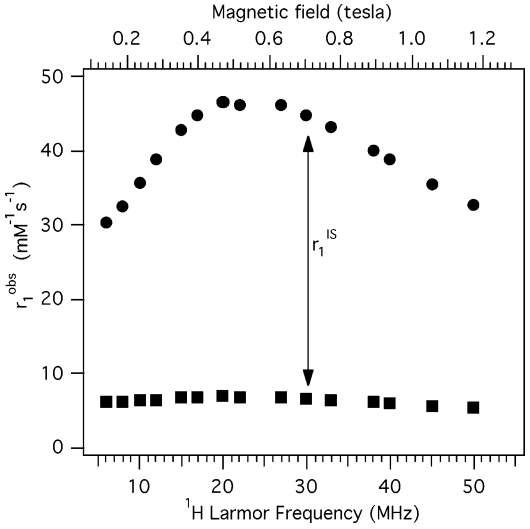

Figure 2. ^{1}H NMRD data at 35 °C for **MnL1** (circles) and **MnL2** (squares) in rabbit serum albumin. The difference in relaxivity is an estimate of the contribution of the inner-sphere water.

the low field data properly requires a more rigorous computational approach taking into account the static ZFS, its degree of rhombicity, and the orientation of the molecular *z* axis with respect to the Mn−H vector. Such an analysis is beyond the scope of this paper. The validity of using the SBM equations and fitting only the high field data was corroborated by some simulations done by Prof. R. Sharp that showed that calculated NMRD profiles with different static ZFS collapse to the SBM curve at high fields and that using the SBM equations above 0.2 T was appropriate for an estimated static ZFS of 0.0686 cm^{-1} (900 G).[60] The high field data were modeled using the SBM equations.[55,56] There are three processes that can contribute to relaxation: electronic relaxation, rotational diffusion, and water exchange. Electronic relaxation ($1/T_{1e}$) for Mn(II) is field dependent, and occurs via a transient zero-field splitting mechanism. This is characterized by Δ^2, the trace of the transient ZFS tensor, and a correlation time for this distortion, τ_v. Rotational diffusion is described by a correlation time, τ_R, and water exchange is defined by the water residency time, τ_m. The NMRD data were collected at four temperatures. Rather than fitting each data set to four parameters, it was assumed that the correlation times had exponential temperature dependencies, and the four data sets were fit simultaneously to seven parameters: three correlation times and their activation energies and the trace of the transient ZFS. Further details and equations used are listed in Supporting Information. The fitting procedure was improved by taking internal motion into account. The Lipari-Szabo formalism[56,57] was applied with a fast local motion having a correlation time less than

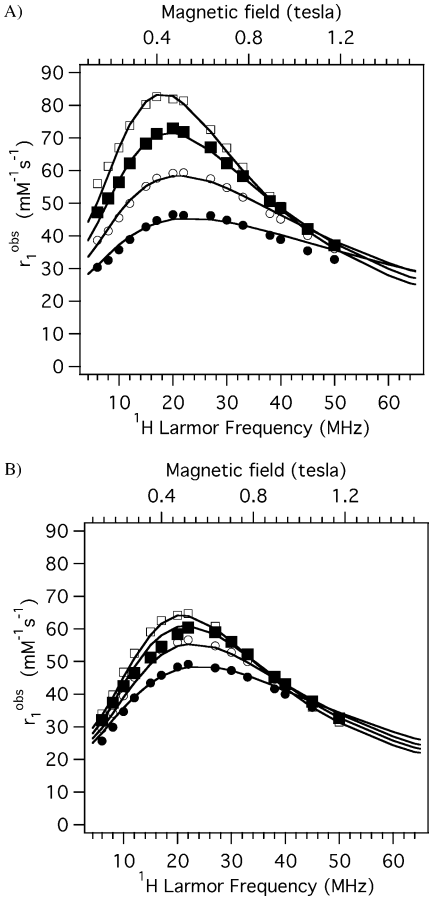

Figure 3. Variable temperature ^{1}H NMRD data (5 °C, □; 15 °C, ■; 25 °C, ○; 35 °C, ●) for **MnL1** in rabbit serum albumin (A) or human serum albumin (B). The solid lines are fits to the data using the parameters in Table 4.

200 ps. This fast motion arises for example from librations within the complex and/or rotation of the bound water molecule. This added an additional parameter, *F*, to the fitting. *F* corresponds to the square of the Lipari-Szabo order parameter.

Since τ_m is so short ($\tau_m \ll T_{1m}$), relaxivity is directly proportional to the relaxation rate, $1/T_{1m}$, of the coordinated water. At the field strengths used here, the terms including the electron Larmor frequency have dispersed, i.e., $\omega_S\tau_c \gg 1$. Moreover, since the local motion is very fast with respect to the global motion, it can be shown that the inner sphere relaxivity simplifies to eq 4

$$r_1^{IS} = \frac{q}{[H_2O]}\frac{1}{T_{1m}} = \frac{q}{[H_2O]}\frac{2}{15}\left(\frac{\mu_0}{4\pi}\right)^2\frac{\gamma_H^2 g_e^2 \mu_B^2 S(S+1)}{r_{MnH}^6}\left[\frac{F3\tau_c}{1+\omega_H^2\tau_c^2}\right] \quad (4)$$

$$\frac{1}{\tau_c} = \frac{1}{\tau_R} + \frac{1}{\tau_m} + \frac{1}{T_{1e}} \quad (5)$$

In Figure 3, the variable temperature NMRD curves of **MnL1** in RSA and HSA are plotted (symbols) along with lines showing the best fit to the model. Figure 3 shows the observed relaxivities versus field, i.e., the measured change in relaxation rate divided by the concentration of **MnL1**.

(55) Toth, E.; Helm, L.; Merbach, A. E. In *Chemistry of Contrast Agents in Medical Magnetic Resonance Imaging*; Toth, E., Merbach, A. E., Eds.; Wiley: New York, 2001; pp 45−119.
(56) Toth, E.; Helm, L.; Merbach, A. E. *Top. Curr. Chem.* **2002**, *221*, 61−101.
(57) Lipari, G.; Szabo, A. *J. Am. Chem. Soc.* **1982**, *104*, 4546−4559.
(58) Kruk, D.; Kowalewski, J. *J. Biol. Inorg. Chem.* **2003**, *8*, 512−518.
(59) Atkins, H. L.; Som, P.; Fairchild, R. G.; Hui, J.; Schachner, E.; Goldman, A.; Ku, T. *Radiology* 1979.
(60) Sharp, R. R.; Personal communication.

Table 4. NMRD Parameters for Fits of the r_1^{IS} Data for **MnL1** at 5, 15, 25, and 35 °C when Bound to RSA or HSA[a]

parameter	RSA	HSA
τ_R^{308} (ns)	15	9.8
ΔE_R (kJ/mol)	1	1
τ_m^{308} (ns)	2.9	5.5
$\Delta H^{\ddagger}$ (kJ/mol)	34.8	37
τ_v^{308} (ps)	22	21
ΔE_v (kJ/mol)	1	1
Δ_t (cm^{-1})	0.0126	0.0154
F	0.76	0.75

[a] The fast local rotational correlation time, τ_{fast}, was fixed at 0.05 ns. The Mn−H distance was assumed to be 2.9 Å.

The solid lines in Figure 3 are the sum of the inner-sphere relaxivity determined from the model above plus the temperature and medium matched relaxivity of **MnL2** (estimate of 2nd sphere and outer-sphere relaxivity). At lower field, T_{1e} is the dominant correlation time and it is limiting relaxivity. As field strength is increased, T_{1e} (and τ_c) also increases and this causes relaxivity to increase. At higher fields, the condition $\omega_H\tau_c > 1$ is met, the denominator in eq 3 becomes large, and relaxivity decreases.

The fitted parameters are listed in Table 4. The NMRD curves can be modeled quite well with water exchange parameters similar to that obtained for the complex in the absence of protein (the ^{17}O study). A result of the fast water exchange is that the water residency time, τ_m, is a dominant contributor to τ_c at higher fields. For relaxivities at 30 MHz, the fast water exchange rate actually limits relaxivity, although at 65 MHz, the common clinical imaging frequency, the relaxivities are similar at all temperatures and water exchange is not limiting. Since $\tau_m < \tau_R$, the rotational correlation time contributes less to the overall correlation time and thus is not well defined (see eq 5). However, it is clear that τ_R is long (values in Table 4 are lower limits), as expected for a complex associated with a large protein.

NMRD data were also reported for the [Mn(EDTA(BOM))-$(H_2O)]^{2-}$ and [Mn(EDTA$(BOM)_2)(H_2O)]^{2-}$ complexes, Chart 1, in the presence of HSA. The data were fit in the original study by Aime et al.[43] and later reanalyzed with a different model by Kruk and Kowalewski.[58] It is difficult to compare the fitted parameters since the model used in each of the other two studies differed from the one used here (both used isotropic models of rotation). Based on their NMRD analysis, Aime et al. noted that the water exchange rate seemed to slow upon binding to albumin. This effect was not observed with **MnL1**, which based on site specificity seen with MS-325,[20] probably binds to a different region on albumin (site II, ibuprofen site) than [Mn(EDTA(BOM))$(H_2O)]^{2-}$ (site I, warfarin site).[43] The differences in albumin binding site may explain why water exchange is affected at one complex upon binding to albumin, but not the other. An alternate explanation could be a result of the different model used to fit the data. Lower than expected relaxivity can be accounted for by a slower water exchange rate or by the presence of anisotropic motion. The other analyses used isotropic models of rotation which may have resulted in a longer τ_m to improve the fitting. Interestingly, for all three complexes bound to albumin, the correlation time at high fields is 2−6 ns, suggesting that the differences among the three albumin-bound compounds are mainly present in data interpretation.

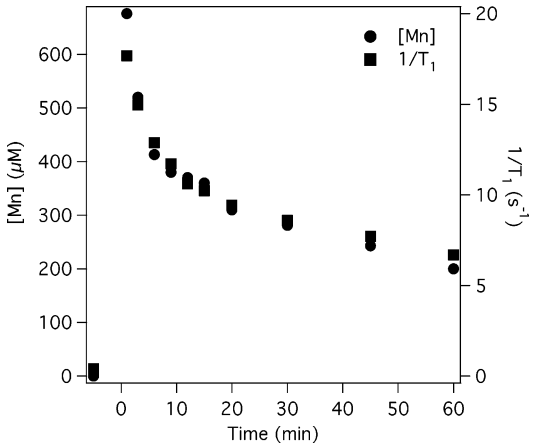

Figure 4. Plasma manganese levels (left axis, ●) in rabbit plasma at various time points, postinjection of 30 μmol/kg of **MnL1**. $1/T_1$ values (right axis, ■) measured ex vivo at 37 °C, 1.4 T correlate with the manganese concentrations.

The variable temperature oxygen and proton relaxation rate studies support the hypothesis that the high relaxivity is a result of a slow tumbling complex with a rapidly exchanging inner sphere water molecule. There is a significant effect arising from relaxation of water(s) in the second coordination sphere as well: up to 20% of r_1^{obs} at 35 °C and up to 30% at 5 °C. Although fast water exchange limits relaxivity at intermediate field strengths (0.5−1 T), at 1.5 T, it is not a limiting factor.

It is also interesting to note that the experimental NMRD curves are different for **MnL1** in either rabbit or human serum albumin. This is mainly manifested in the fits as slightly different water exchange rates (slower for HSA) and a slightly faster electronic relaxation rate for **MnL1** in the presence of HSA. It is not clear at the moment why the different species albumins yield different relaxation behavior. This should be further studied.

The behavior of **MnL1** was further evaluated in a rabbit model. A pilot pharmacokinetic study demonstrated that **MnL1** persists in the blood of a rabbit, at least out to 1 h. Figure 4 shows the change in plasma manganese levels as a function of time after an intravenous injection of a 30 μmol/kg dose of **MnL1**. Based on this pilot study, the plasma half-life is 30 min. Although no chemical speciation studies were done, it is likely that the manganese remains chelated to **L1**. In comparison, the half-life of Mn(II) when given as $MnCl_2$ solution is 0.8 min in plasma.[59] The T_1 of each plasma sample was measured at 60 MHz, 37 °C and the $1/T_1$ rates are plotted in Figure 4 on the right axis (note the scales for the manganese concentration and the relaxation rates are different). Figure 4 also shows that the change in relaxation rate with time mirrors that of the change in manganese concentration. The observed relaxivity determined from this data ranges from 25.5 mM^{-1} s^{-1} at 1 min (650 μM Mn) to 31.4 mM^{-1} s^{-1} at 60 min (37 °C, 1.4 T, 60 MHz). The fraction bound to albumin is obviously concentration dependent, and relaxivity is expected to decrease as the concentration of

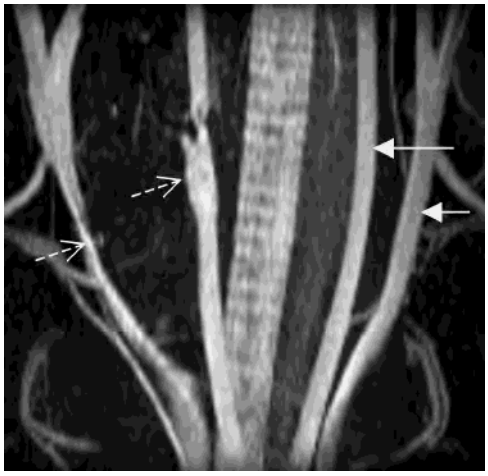

Figure 5. Figure 5 is a coronal maximum intensity projection (MIP) image of the ventral neck region of a rabbit following i.v. administration of 10 μmol/kg **MnL1**. The dashed arrows denote regions of vessel damage in the right jugular vein and right carotid artery; the solid arrows show no damage in the contra lateral vessels.

agent increases (more free fraction present). The ex vivo numbers are in very good agreement with relaxivities determined by adding **MnL1** to rabbit plasma ($r_1^{obs} = 32$ mM^{-1} s^{-1}, 92 μM Mn, 37 °C, 1.4 T, 60 MHz). The similarity in relaxivity suggests that the complex remains intact in plasma over this time period. This may be expected based on the relatively large formation constant ($10^{13.9}$)[61] for $[Mn(EDTA)(H_2O)]^{2-}$. The T_1 data also demonstrate that **MnL1** should be quite effective for imaging the rabbit blood pool either under dynamic (immediately postinjection) or steady-state conditions at this dose. Even at 60 min postinjection, on a T_1-weighted image, the blood should appear brighter than any other tissue.

To further test the ability of **MnL1** to function as a contrast agent, MR imaging studies were performed at 30 μmol/kg in New Zealand white rabbits. **MnL1** showed good delineation of the blood vessels at this dose. The dose was subsequently lowered to 10 μmol/kg and good vascular images were still obtained. Figure 5 is a coronal maximum intensity projection (MIP) image of the ventral neck region of a rabbit following i.v. administration of 10 μmol/kg **MnL1**. The carotid artery and jugular vein on the left side of the image were injured prior to contrast agent administration in order to induce thrombus formation. The difference between the normal (solid arrows) and injured (dashed arrows) vessels is clear from the image. The carotid artery is inflamed at the site of injury and the suture distal to the thrombus is visible. The jugular vein on left shows marked stenosis. The contrast-to-noise ratio (CNR) was measured by comparing the blood intensity in the normal vessel with that in surrounding muscle. For five animals imaged at eight minutes postinjection, the CNR was 30.7 ± 4.6 ($N = 5$).

During the pharmacokinetic study and the imaging studies, cardiac function was monitored by measuring blood pressure and heart rate. In some studies, electrocardiograms were also acquired. At either the 10 or 30 μmol/kg dose, there was no observable effect on cardiac function. Unchelated manganese(II) is known to have an acute cardiac toxicity; the absence of any acute cardiac toxicity suggests that the manganese remains predominantly associated with the **L1** ligand. Future work will address the question of speciation of the agent in plasma and its biodistribution.

Conclusion

This work supports the potential use of Mn(II) complexes as MRI contrast agents. **MnL1** exhibits high relaxivity in plasma due to slow tumbling of the complex when associated with serum albumin coupled with fast exchange of the inner sphere water. Binding to serum albumin kept the complex in the blood and allowed high-resolution imaging of blood vessels. In a rabbit model, images were obtained with good contrast-to-noise ratio, and it was possible to distinguish normal vs injured vessels resulting from stenosis and inflammation. Although no acute cardiotoxicity was observed, additional studies on in vivo stability and toxicity are necessary. These results indicate that Mn(II)-based complexes may be useful as the basis for high relaxivity MRI contrast agents.

Acknowledgment. The referees are thanked for their thorough comments and useful suggestions.

Supporting Information Available: Theory used to extract molecular parameters from O-17 and NMRD data, tables of observed relaxivity for **MnL1** and **MnL2** as a function of field and temperature in RSA and HSA, HPLC-MS data for **MnL1**. This material is available free of charge via the Internet at http://pubs.acs.org.

IC049559G

(61) Martell, A. E.; Smith, R. M.; *Critical Stability Constants*; Plenum: New York, 1974; Vol. 1.